

OPTICS AND CLOAKING IN FDTD

by

Maksim Sipos

A senior thesis submitted to the faculty of

Ithaca College

in partial fulfillment of the requirements for the degree of

Bachelor of Science

Department of Physics

Ithaca College

April 2008

Copyright © 2008 Maksim Sipos

All Rights Reserved

ITHACA COLLEGE

DEPARTMENT APPROVAL

of a senior thesis submitted by

Maksim Sipos

This thesis has been reviewed by the research advisor, senior thesis instructor, and department chair and has been found to be satisfactory.

Date

Bruce G. Thompson, Advisor

Date

Luke Keller, Senior Thesis Instructor

Date

Bruce G. Thompson, Chair

ABSTRACT

OPTICS AND CLOAKING IN FDTD

Maksim Sipos

Department of Physics

Bachelor of Science

Finite difference time domain (FDTD) method can be used to model classical electromagnetic systems. We show that the FDTD simulation yields the fundamental optical phenomena such as reflection, refraction, interference and diffraction. FDTD systems can also be used to accurately model the behavior of anisotropic materials, through a suitable modification of the field arrangement. We demonstrate the bending of a TM wave around a perfectly conducting cylinder by a layer of anisotropic material. This effect can be used to effectively conceal or "cloak" objects with such layers.

ACKNOWLEDGMENTS

The author thanks Ithaca College for its support through the Dana Fellowship Program. The author also recognizes the helpful editing comments of Luke Keller and an anonymous editor at the American Journal of Physics. The author would particularly like to acknowledge his advisor, Professor Bruce G. Thompson, for the many hours spent working together on this research.

Contents

| | |
|---|------------|
| Table of Contents | vii |
| 1 Theory | 1 |
| 1.1 Introduction | 1 |
| 1.2 The Yee algorithm | 2 |
| 1.3 Divergence in the Yee algorithm | 4 |
| 1.4 Computational Methods | 6 |
| 1.5 Grid boundary issues | 8 |
| 1.6 Numerical dispersion | 10 |
| 2 Simulations | 13 |
| 2.1 One Dimension | 13 |
| 2.2 Optical simulations | 14 |
| 2.3 Tensor material properties | 16 |
| 2.4 Bending wavefronts: cloaking | 17 |
| 2.5 Conclusions | 20 |
| A Yee Algorithm Derivation in 3D | 25 |
| B Complete Update Equations | 27 |
| C Divergence Free Nature in 3D | 29 |
| Bibliography | 31 |

Chapter 1

Theory

1.1 Introduction

The discovery of Maxwell's equations, at the end of the 19th century, succeeded in completely explaining electromagnetic phenomena. However, the problem of analytically solving the equations for complex electromagnetic interactions persisted. The nature of Maxwell's equations made it only possible to solve them for special cases. In 1966, Yee described how approximating the derivatives in Maxwell's equation with finite differences can be used to simulate electromagnetic interactions. Yee's algorithm, now known as the basis of the Finite Difference Time Domain (FDTD) is powerful because it is applicable to any physical situation. It describes successfully a wide range of material properties and systems with arbitrary geometry [1]. Yee algorithm's versatility brought a great deal of attention to FDTD. Many useful boundary conditions and incident wave schemas are known today.

We show how FDTD can be used to simulate anisotropic materials, through a change in the field arrangement and the updating formulas. Following the work of Ward [3] and Pendry [4], we describe how anisotropic materials can be used to guide

the power lines of EM waves. This makes a unique application possible: construction of a "cloak" around a visible object that makes all incident rays bend and pass around the object making it virtually invisible. We show simulations of this effect and describe it qualitatively.

In Section 1.2 we describe Yee's algorithm for the simplest case of a nonconducting, linear and isotropic medium with no free currents and no free charges. In Section 1.3 we show how Yee's model is consistent with Gauss's law for electric and magnetic fields. In Section 1.4 we describe the details related to our computational implementation. In Section 1.5 we explain that special care must be taken when choosing the boundary conditions when for Yee's algorithm. We describe in Section 1.6 the ways to combat numerical dispersion that is inherent in FDTD. We give an in-depth analysis of the finite-difference scheme in one dimension in Section 2.1. We give simulations of some optical phenomena in Section 2.2. In Section 2.3 we describe the generalization of the Yee's algorithm to anisotropic materials, and in Section 2.4 we describe a simulation that shows how such a method could be used to create electromagnetic "cloaking devices". This thesis also includes a number of electronic resources that are available at the EPAPS repository. [2]

1.2 The Yee algorithm

The behavior of classical electromagnetic phenomena is determined by Maxwell's equations. In a linear, isotropic non-conductive medium with no free charge or cur-

rents, they are:

$$\frac{\partial \mathbf{B}}{\partial t} = -\nabla \times \mathbf{E}, \quad (1.1)$$

$$\frac{\partial \mathbf{D}}{\partial t} = \nabla \times \mathbf{H}, \quad (1.2)$$

$$\nabla \cdot \mathbf{B} = 0, \quad (1.3)$$

$$\nabla \cdot \mathbf{D} = 0, \quad (1.4)$$

where the constitutive relations in the simplest case are $\mathbf{B} = \mu \mathbf{H}$ and $\mathbf{D} = \epsilon \mathbf{E}$. Simulation of electromagnetic waves is made possible by creating a cubic lattice and assigning a staggered arrangement of \mathbf{E} and \mathbf{H} components to the nodes. [1] (See Figure 1.1.) This arrangement allows for an easy calculation of curl terms in the equations. Sometimes it is also useful to model free currents in the medium. In that case Equation (1.2) may be replaced by

$$\frac{\partial \mathbf{D}}{\partial t} = \nabla \times \mathbf{H} - \mathbf{J}_f. \quad (1.5)$$

The finite difference substitutions that follow are only slightly more complex when the \mathbf{J}_f term is non-zero.

In this document we limit our simulations to systems with no variation in the z direction and thus Maxwell's equations can be separated into two 2-D modes. The transverse magnetic mode (TM) has $E_x = E_y = H_z = 0$ and the transverse electric mode (TE) has $H_x = H_y = E_z = 0$. Arrangements of components corresponding to those given in Figure 1.1 for a 2-D case are simply planes of the Yee cube defined by $z = \text{const}$. Figure 1.2 shows the nodes and field components of the slice at $z = k\Delta x$, which corresponds to the TM mode. Notice that E_z is appropriately surrounded by the H_x and H_y components making the first-order difference of the curl easy to evaluate. The slice at $z = (k + 1/2)\Delta x$ corresponds to the TE mode.

Following Yee [1], we will use the notation that $E_z^n(i, j, k)$ represents the magnitude of z -component of \mathbf{E} at $(i \Delta x, j \Delta x, k \Delta x)$, at time $n \Delta t$. Note that the lattice is cubic

and so the distance increments in each direction are equal. Using finite differences for space and time, with the arrangement given in Figure 1.2 we can approximate Equations (1.1) and (1.2) for a TM wave by

$$E_z^n(i, j) = E_z^{n-1}(i, j) + \frac{1}{\epsilon} \frac{\Delta t}{\Delta x} \cdot \left[\begin{array}{l} \left(H_y^{n-\frac{1}{2}}(i+\frac{1}{2}, j) - H_y^{n-\frac{1}{2}}(i-\frac{1}{2}, j) \right) \\ - \left(H_x^{n-\frac{1}{2}}(i, j+\frac{1}{2}) - H_x^{n-\frac{1}{2}}(i, j-\frac{1}{2}) \right) \end{array} \right] \quad (1.6)$$

$$H_x^{n+\frac{1}{2}}(i, j+\frac{1}{2}) = H_x^{n-\frac{1}{2}}(i, j+\frac{1}{2}) - \frac{1}{\mu} \frac{\Delta t}{\Delta x} (E_z^n(i, j+1) - E_z^n(i, j)), \quad (1.7)$$

$$H_y^{n+\frac{1}{2}}(i+\frac{1}{2}, j) = H_y^{n-\frac{1}{2}}(i+\frac{1}{2}, j) + \frac{1}{\mu} \frac{\Delta t}{\Delta x} (E_z^n(i+1, j) - E_z^n(i, j)). \quad (1.8)$$

The equations are set up in a leap-frog manner in time. In order to calculate \mathbf{E} at time n , one uses \mathbf{H} at time $n - \frac{1}{2}$. Similarly, to calculate \mathbf{H} at time $n + \frac{1}{2}$, one uses \mathbf{E} at time n . A complete derivation of Equations 1.6, 1.7 and 1.8 for a general case in three dimensions is given in Appendix A. Complete update equations for the case of three dimensions are given in Appendix B. To ensure numerical stability in two dimensions the time step is limited to: [7]

$$\Delta t \leq \frac{\Delta x}{v_{max} \sqrt{2}}, \quad (1.9)$$

where $v_{max} = \sqrt{1/\epsilon\mu}$ is the maximum propagation speed.

1.3 Divergence in the Yee algorithm

The Maxwell divergence equations (1.3) and (1.4) are not needed for timestepping, but are satisfied by the Yee lattice. To illustrate, consider equation (1.3) for a TM mode. In two dimensions the flux is calculated as flow across a boundary line. Let Φ be the magnetic flux through the square shown by the dotted line in Figure 1.2. Then,

$$\Phi = \Delta x \mu \left(H_x(i+1, j+\frac{1}{2}) - H_x(i, j+\frac{1}{2}) + H_y(i+\frac{1}{2}, j+1) - H_y(i+\frac{1}{2}, j) \right). \quad (1.10)$$

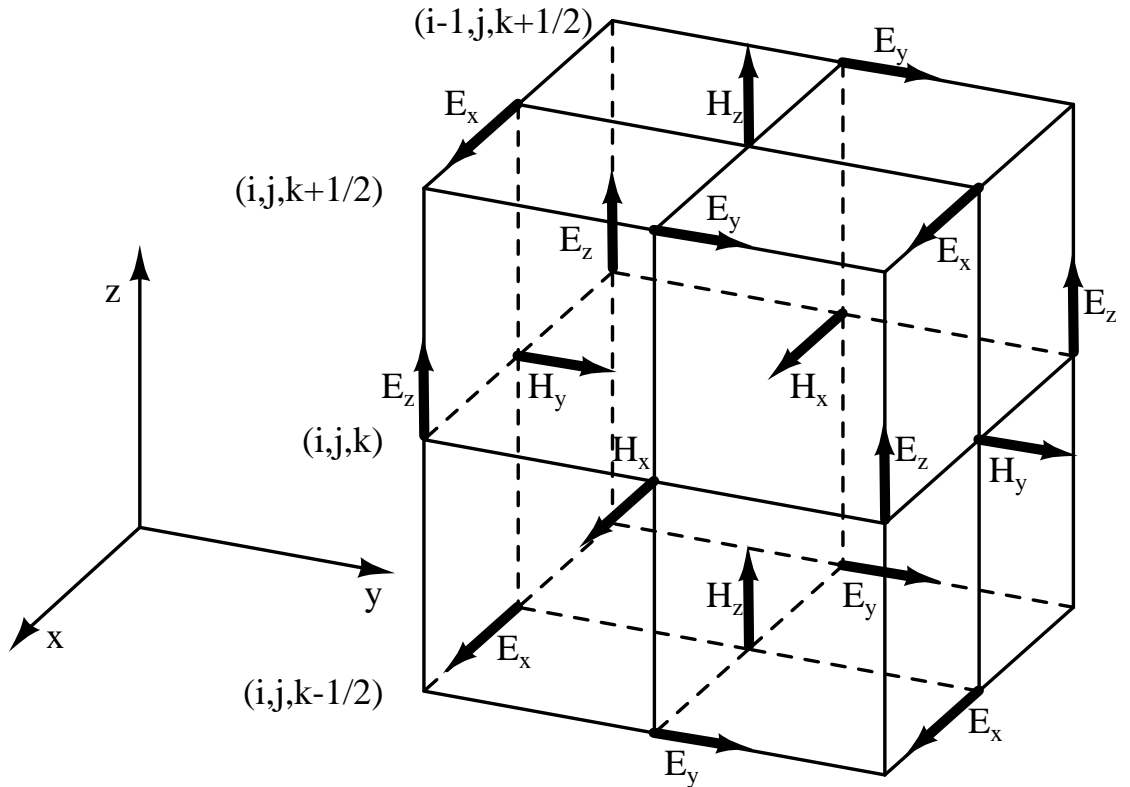


Figure 1.1 Yee's arrangement of field components in a cubic lattice. Each field component is surrounded by the components necessary to calculate the curl terms in Equations (1.1) and (1.2). For instance, H_x has E_z in the y direction and E_y in the z direction. The Yee lattice can be seen as a mesh of interlinked loops of magnetic or electric fields. Also notice that the $z = k\Delta x$ plane, for integer k represents the arrangement of field components appropriate for a 2-D TM system and the $z = (k + \frac{1}{2})\Delta x$ plane represents the arrangement of components for a 2-D TE system.

The time derivative of Φ rendered into finite differences yields finite difference terms in H_x and H_y . When equations 1.7 and 1.8 are substituted for these terms, all terms cancel, therefore $\partial\Phi/\partial t = 0$. Since we assume that the flux is zero at the start, it never departs from zero. This procedure can be generalized to show that the fields satisfy the divergence equations in three dimensions. [8] We show that the magnetic field satisfies the divergence requirements in Appendix C.

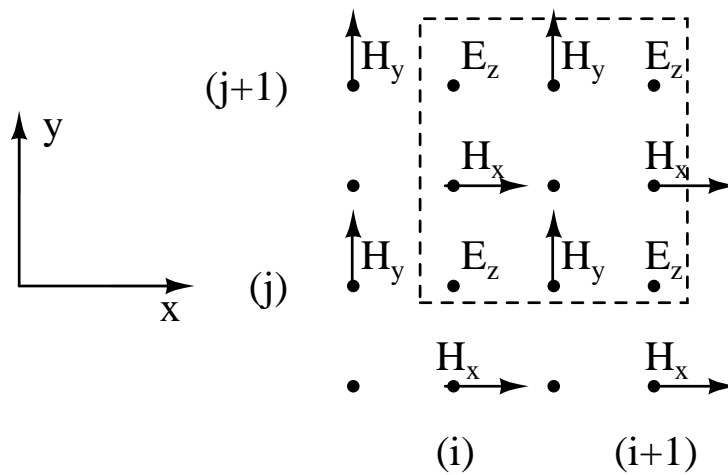


Figure 1.2 The arrangement of field components on a 2-D grid for the TM mode. E_z is out of the page. The dotted lines define a boundary for the calculation of the divergence.

1.4 Computational Methods

The code to perform the simulations given in this paper operates in the following way:

1. Memory is allocated for all necessary E and H fields, and material properties ϵ and μ spread across the $X \times Y \times Z$ grid points. Depending on the grid boundary technique used, two or more data points are kept for each field component. One

is used for the values of fields after the latest time-step n or $n + \frac{1}{2}$ in the calculation. Others represent previous values of the fields, that is, those after the time-step $n - k$ or $n - k + \frac{1}{2}$, for integer $k > 0$. For the first-order finite difference algorithm given in Section 1.2, keeping one grid of “historical” values is sufficient. However, some boundary conditions (such as the Mur absorbing boundary condition given in Section 1.5) require higher order finite-differences, and keeping multiple grids of “historical” field values.

2. Constants defining the medium are initialized in some geometric pattern. Depending on the position (x, y, z) in the grid, the values of ϵ and μ are set accordingly.
3. Fields are set to wanted initial conditions. There are two possibilities:
 - (a) The incident waves are introduced continuously into the simulation while it is running. In that case, in this step we set the fields to 0 everywhere. As an example of this, consider the simulation of the two-slit interference in Section 2.2.
 - (b) Alternatively, we initialize the fields in the simulation to some non-zero arrangement. For example, we can construct a Gaussian plane wave with amplitude $E = 1.0$, $H = 1.0/c$ where c is the speed of light in the medium. An example of this is the initial Gaussian plane wave used in the reflection simulation in Section 2.2.
4. Steps 5 through 7 are performed as many times as wanted for the simulation, or until the simulation is numerically valid.
5. We perform this step if we are going to introduce the incident fields in the way described in Step 3(a). Values of the fields at the boundary are set to equal

a function of the time step n . For instance, the left boundary of the grid of E fields may be set to $\sin(n/\omega)$, thereby introducing a plane wave into the simulation continuously.

6. Calculation of the H fields is performed. Resultant H fields are used to calculate the E fields.
7. “Histories” of the fields are “propagated”. In other words, the grid corresponding to time step $n - k - 1$ is set to equal to the grid corresponding to the time step $n - k$. In this way, sufficient number of previous grids is kept in memory, available for the Yee algorithm.

Particular attention must be made to efficiently perform steps 5 through 7. For a simulation of length T time-steps, step 5 contributes at most $O(XYZT)$ operations to the running time of the program, for an $X \times Y \times Z$ grid. Step 6 contributes on the order of $O(XYZT)$ to the running time of the program. Finally, step 7 can be made to correspond to a few pointer or reference reassignments, contributing $O(T)$ to the running time of the program.

1.5 Grid boundary issues

FDTD grids cannot be infinite because computer memories are finite. Boundary conditions must be set up carefully at the grid edges. A simple boundary condition in FDTD is the perfectly conducting plane. We set $E_{\parallel} = 0$ and $H_{\perp} = 0$ at that plane. Let the edges of our TM grid be $x = 0$, $x = X\Delta x$, $y = 0$ and $y = Y\Delta x$, with the field components arranged in the lattice given by Figure 1.2. Then, perfectly conducting boundary condition amounts to setting $E_z = 0$ and $H_x = 0$ at $x = 0$ and $x = X\Delta x$, and $E_z = 0$ and $H_y = 0$ at $y = 0$ and $y = Y\Delta x$ boundaries. Propagating an infinite

plane wave strictly along the x direction is done by setting $H_x = 0$ at the boundaries defined by $y = 0$ and $y = Y\Delta x$.

In some of the simulations we use an absorbing boundary condition (ABC) on the grid edges. When an incident wave impacts the boundary, these ABCs attempt to minimize any reflections that arise. The Mur boundary condition that we use relies on the fact that each field component W satisfies the two-dimensional scalar wave equation

$$(\partial_x^2 + \partial_y^2 - c_0^{-2}\partial_t^2)W = 0. \quad (1.11)$$

Defining the partial differential operator

$$G \equiv \frac{\partial^2}{\partial x^2} + \frac{\partial^2}{\partial y^2} - \frac{1}{c^2} \frac{\partial^2}{\partial t^2} \equiv D_x^2 + D_y^2 - \frac{1}{c^2} D_t^2 \quad (1.12)$$

lets us write the scalar wave equation as

$$GW = 0. \quad (1.13)$$

The G operator can be algebraically factored into

$$GW = G^+G^-W = 0, \quad (1.14)$$

where

$$G^+ \equiv D_x - \frac{D_t}{c} \sqrt{1 - s^2}, \quad (1.15)$$

$$G^- \equiv D_x + \frac{D_t}{c} \sqrt{1 - s^2}, \quad (1.16)$$

$$s \equiv \frac{D_y}{D_t/c}. \quad (1.17)$$

Engquist and Majda [6] showed that the equations G^+W and G^-W correspond to *one-way wave equations* for waves propagating in $+x$ and $-x$ directions, respectively.

Then appropriate boundary condition along the x direction is

$$G^-W \Big|_{x=0} = 0, \quad (1.18)$$

$$G^+W \Big|_{x=X\Delta x} = 0. \quad (1.19)$$

Similar derivation can be used to construct boundary conditions for components of waves travelling in the y direction. Mur used a second-order Taylor expansion of Equations 1.18 and 1.19 to construct ABCs suitable for FDTD. [5] Other boundary conditions that absorb incoming waves are also possible. [8]

1.6 Numerical dispersion

The Yee algorithm produces dispersion of waves even in regions of simulated free space. As Taflove and Hagness [8] state:

An intuitive way to view this phenomenon is that the FDTD algorithm embeds the electromagnetic wave interaction structure of interest in a tenuous “numerical ether” having properties very close to vacuum, but not quite. This “ether” causes propagating numerical waves to accumulate delay or phase errors that can lead to nonphysical results.

That is, the Yee grid itself is a dispersive anisotropic medium.

Attention must be paid to the grid increment size, Δx , in relation to the minimum wavelength, λ_{min} , of the simulated wave. The fields should not vary too much with each grid step or else the first-order difference approximation used in the Yee algorithm will not accurately reflect the true field derivative and there will be dispersion in the system. Setting $\Delta x = \lambda_{min}/29$ produces less than 0.1% dispersion and commonly used grid resolutions are between $\lambda_{min}/10$ and $\lambda_{min}/40$. [8]

Further, a numerical wave in the Yee lattice has a propagation velocity that depends on the direction of propagation. For example, Taflove and Hagness [8] show that, for a 2-D grid with a time step of $\Delta t = \Delta x/2c$ and grid spacing of $\Delta x = \lambda_0/20$ (λ_0 is the wavelength of the incident wave), the numerical phase speed along the direction of the grid is $0.9969c$, whereas along the diagonal it is the slightly faster speed

of $0.9990c$. Note that both of these are slower than the desired numerical speed, c . This shortfall and anisotropy of about 0.3% can be reduced, if needed, by reducing the grid size. Another way to mitigate the anisotropy, at least in two dimensions, is to use a hexagonal grid. [9] The grid equations are only slightly more complex but produce a reduction in anisotropy by a factor of about 64. Many of the recent advances in FDTD simulations are a result of using a variety of other nonuniform grids. [8]

Chapter 2

Simulations

2.1 One Dimension

One way to see how the interlinked field difference equations lead to wave motion is to look at the simplest possible system. Assume that we have the one dimensional system at $y = j\Delta x$ of Figure 1.2 and that the initial fields E_z^0 and $-H_y^0$ are single Gaussian pulses along the x direction. Note that, as described above, the grid should have a spacing which is much less than the width of the pulse. Then we expect that time stepping will show the pulses traveling in the $+x$ direction. Since there is no variation of E_z in the y direction, no H_x will be generated by Equation 1.7. Equations (1.6) and (1.8) become:

$$E_z^n(i) = E_z^{n-1}(i) + \frac{1}{\epsilon} \frac{\Delta t}{\Delta x} \left(H_y^{n-\frac{1}{2}}(i+\frac{1}{2}) - H_y^{n-\frac{1}{2}}(i-\frac{1}{2}) \right) \quad (2.1)$$

$$H_y^{n+\frac{1}{2}}(i+\frac{1}{2}) = H_y^{n-\frac{1}{2}}(i+\frac{1}{2}) + \frac{1}{\mu} \frac{\Delta t}{\Delta x} (E_z^n(i+1) - E_z^n(i)). \quad (2.2)$$

These can easily be entered into a spreadsheet and time stepped. An example spreadsheet is available in EPAPS. [2] The peak magnitudes of the fields are seen to move in the expected direction. Since the grid is necessarily coarse, numerical noise is also

generated.

2.2 Optical simulations

In two dimensions the method can simulate several optical phenomena. Videos of these simulations are available at EPAPS. [2] Consider initial E_z and H_y pulses which are Gaussian in the x direction and which have a finite extent in the y direction. The y direction is truncated smoothly using Gaussian tails. For normal incidence on a barrier extending in the y direction, the field magnitudes are given by

$$\Psi(x, y) = \exp\left(-\frac{x^2}{2\sigma_x^2}\right) \Upsilon(y), \quad (2.3)$$

where $\Upsilon(y)$ is a ‘‘plateau’’ function with Gaussian tails defined by

$$\Upsilon(y) = \begin{cases} \exp\left(-\frac{(y-y_1)^2}{2\sigma_y^2}\right) & \text{for } y < y_1, \\ 1 & \text{for } y_1 \leq y \leq y_2, \\ \exp\left(-\frac{(y-y_2)^2}{2\sigma_y^2}\right) & \text{for } y > y_2. \end{cases} \quad (2.4)$$

and σ_x and σ_y define the width of the Gaussian pulse and tail. We use $\Upsilon(y)$ to laterally constrain our incident wave to minimize the interaction with boundaries. To simulate non-normal incidence on the barrier, these fields are rotated by an angle θ . This yields the initial TM field components,

$$E_z^0(x, y) = \Psi(x', y'), \quad (2.5)$$

$$H_y^0(x, y) = \frac{1}{Z} \Psi(x', y') \cos \theta, \quad (2.6)$$

$$H_x^0(x, y) = \frac{1}{Z} \Psi(x', y') \sin \theta. \quad (2.7)$$

where $Z = \sqrt{\mu_0/\epsilon_0}$, θ is the angle of incidence and the primes indicate that the original function has been rotated away from normal incidence. The initial E_z^0 field is shown at location A in the left diagram of Figure 2.1 superimposed on the result

of the simulation. With these initial fields, we expect the wave to travel upward along the line of incidence. The boundary on the left side is perfectly conducting. As shown at location B of Figure 2.1, we observe the expected reflected wave, that is, the electric field is inverted (dark shading is negative) and at a reflected angle equal to the incident angle. The remainder of the incident pulse is seen at location C .

One additional feature seen in the simulation result is that the reflected wave at C has an arc extending from the right end. This is a real (not computational) diffractive effect due to the truncation of the left side of the original pulse. Whenever a wave is truncated, whether is be due to a barrier or, as in this case, the initial field, there will be diffraction from that edge.

We also consider the phenomenon of double slit diffraction and interference. Our incident wave is a continuous sinusoidal plane wave propagating in the $-x$ direction. We introduce the wave into our grid by varying E_z at $x = X\Delta x$ edge,

$$E_z^n(X, y) = A \sin(\omega n \Delta t). \quad (2.8)$$

Our result is illustrated in the upper right of Figure 2.1. Here we used absorbing boundary conditions on the edges as described by Mur. [5] As expected, there is a central interference peak with flanking intensity peaks to either side. Note that the peak intensities correspond to both the maxima and minima (light and dark) of the E_z field. For narrow slits, these should be at an angle given by $\sin \theta = n\lambda/d$, which in this case is at $\theta = 17$ deg. The tick marks on the figure show this to be the case.

Properties ϵ and μ in Equations (1.6), (1.7) and (1.8) may also be functions of x and y . In the illustration on the lower right of Figure 2.1, a symmetric lens is constructed with radius of curvature R and with an ϵ that gives index of refraction of 1.5. The lensmaker's formula with this index gives a focal length of $f = R$. Indeed, the simulation shows a wave that is focused at approximately the radius of curvature

of the lens.

2.3 Tensor material properties

Although not shown here, Yee included the possibility of conductivity changes in the modeled material. The method can also be extended to include tensor forms of the material properties. [10, 11] Here we extend the 2-D *TM* difference equations to include tensor forms for ϵ and μ for nonconductive materials.

The constitutive relations become

$$\begin{pmatrix} B_x \\ B_y \end{pmatrix} = \begin{pmatrix} \mu_{xx} & \mu_{xy} \\ \mu_{xy} & \mu_{yy} \end{pmatrix} \begin{pmatrix} H_x \\ H_y \end{pmatrix}. \quad (2.9)$$

and $D_z = \epsilon_{zz}E_z$. After substituting this relation into Equation (1.1) and solving for the time derivatives, we obtain

$$\frac{\partial H_x}{\partial t} = -\frac{1}{\mu_{xx}\mu_{yy} - \mu_{xy}^2} \left(\mu_{yy} \frac{\partial E_z}{\partial y} + \mu_{xy} \frac{\partial E_z}{\partial x} \right), \quad (2.10)$$

$$\frac{\partial H_y}{\partial t} = \frac{1}{\mu_{xx}\mu_{yy} - \mu_{xy}^2} \left(\mu_{xx} \frac{\partial E_z}{\partial x} + \mu_{xy} \frac{\partial E_z}{\partial y} \right). \quad (2.11)$$

Notice that the off-diagonal permeability terms create a new link to $\partial H_x/\partial t$ via $\partial E_z/\partial x$ and similarly for $\partial H_y/\partial t$ via $\partial E_z/\partial y$. The Yee lattice of Figure 1.2 does not have values at the proper nodes to calculate these spatial differences. However, the nodes can be filled by averaging the four values of E_z surrounding the desired one. Therefore we introduce \overline{E}_z at these locations.

$$\overline{E}_z^n(i + \frac{1}{2}, j + \frac{1}{2}) = \frac{1}{4} \cdot \left[\begin{array}{l} E_z^n(i, j) + E_z^n(i+1, j) + \\ E_z^n(i, j+1) + E_z^n(i+1, j+1) \end{array} \right]. \quad (2.12)$$

The update equations then become

$$H_x^{n+\frac{1}{2}}(i, j+\frac{1}{2}) = H_x^{n-\frac{1}{2}}(i, j+\frac{1}{2}) - \frac{1}{\mu_{xx}\mu_{yy} - \mu_{xy}^2} \cdot \begin{bmatrix} \mu_{yy} (E_z^n(i, j+1) - E_z^n(i, j)) + \\ \mu_{xy} (\overline{E}_z^n(i+\frac{1}{2}, j+\frac{1}{2}) - \overline{E}_z^n(i-\frac{1}{2}, j+\frac{1}{2})) \end{bmatrix}, \quad (2.13)$$

$$H_y^{n+\frac{1}{2}}(i+\frac{1}{2}, j) = H_y^{n-\frac{1}{2}}(i+\frac{1}{2}, j) + \frac{1}{\mu_{xx}\mu_{yy} - \mu_{xy}^2} \cdot \begin{bmatrix} \mu_{xx} (E_z^n(i+1, j) - E_z^n(i, j)) + \\ \mu_{xy} (\overline{E}_z^n(i+\frac{1}{2}, j+\frac{1}{2}) - \overline{E}_z^n(i+\frac{1}{2}, j-\frac{1}{2})) \end{bmatrix}, \quad (2.14)$$

with the finite difference equation (1.6) remaining virtually unchanged except for the substitution $\epsilon = \epsilon_{zz}$.

2.4 Bending wavefronts: cloaking

Recently, Pendry *et al.* [4] have shown that, by using coordinate transformations to determine material properties, electromagnetic fields can be redirected at will. For propagating fields, the idea is to imagine a spatial distortion of a uniform vector field which would mimic the desired bending of the Poynting vector. Then construct a coordinate transformation from, for instance, a cartesian system to a system which produces this spatial distortion. Maxwell's equations have the same form in the new coordinate system provided the fields and permittivity and permeability are scaled appropriately. [3] The permittivity and permeability may also become tensors. These transformed property values produce the desired redirection of the Poynting vector. The values needed may be zero, infinite or negative and so may not be physically reasonable. However, the ability to construct metamaterials [12] with a wide range of material properties has begun to make this possibility real.

One such transformation is to bend a wavefront around a region thus rendering

anything interior to that space invisible. Here we use the tensor formulation from the previous section to illustrate the cloaking phenomenon in two dimensions. Assume that the region to be cloaked is a cylinder with radius R_1 that is surrounded by a region of radius R_2 containing altered material properties. The required relative permittivity and permeability values to bend the wavefront around R_1 are given in cylindrical coordinates by: [13]

$$\epsilon_r = \mu_r = \frac{r - R_1}{r}, \quad \epsilon_\phi = \mu_\phi = \frac{r}{r - R_1}, \quad (2.15)$$

$$\epsilon_z = \mu_z = \left(\frac{R_2}{R_2 - R_1} \right)^2 \frac{r - R_1}{r}. \quad (2.16)$$

where r is the distance from the center of the cylindrical object. Assuming an incoming TM plane wave in the $+x$ direction, a 2nd rank tensor transformation gives the following cartesian tensor elements:

$$\epsilon_{zz} = \epsilon_0 \epsilon_z, \quad (2.17)$$

$$\mu_{xx} = \mu_0 (\mu_r \cos^2 \phi + \mu_\phi \sin^2 \phi), \quad (2.18)$$

$$\mu_{xy} = \mu_{yx} = \mu_0 (\mu_r - \mu_\phi) \sin \phi \cos \phi, \quad (2.19)$$

$$\mu_{yy} = \mu_0 (\mu_r \sin^2 \phi + \mu_\phi \cos^2 \phi). \quad (2.20)$$

With this form of μ_{xx} , μ_{xy} and μ_{yy} , the factor $\mu_{xx}\mu_{yy} - \mu_{xy}^2$ in Equations (2.10) and (2.11) and Equations (2.13) and (2.14) becomes simply μ_0^2 . Figure 2.2 shows the spatial variation of the tensor properties. It is apparent that extreme values of the material properties are needed and that they have large gradients.

The extreme property values require that some care is needed in the calculations. As described in the first section, numerical stability requires that the time step is smaller than the spatial step divided by a factor times the local phase speed. When μ or ϵ goes to zero, the phase speed gets very large, rendering stability impossible. Therefore μ and ϵ must be kept above predetermined minimum values so that the

time step is reasonable. A phase speed that exceeds the speed of light in a vacuum is allowed provided that the group velocity does not. The group velocity is slower than the phase velocity if the material is dispersive. Therefore, this system is necessarily dispersive. [4] The infinite property values also create difficulties in calculations and so are limited in their maximum values. These compromises in property values mean that the numerical simulation will not show an ideal cloak of the interior region. A real material will have an even less ideal ability.

To observe the effect of the cloaking region, we construct a continuous incident wave impinging on a perfectly conducting cylinder with and without a cloaking region. The results of our simulation are shown in Figure 2.3. The cloak has the desired effect of reconstructing the wavefront beyond the cylinder. The result is not perfect but there is a considerable reduction in the disturbance to the field both down stream (to the right) and upstream (i.e. reflections). Also note that there has also been a small amount of scattering by the cloaked conducting cylinder as expected from the compromises made in the material values.

Some feeling for how the wavefront is turned can be gotten by looking at the μ_{xy} diagram of Figure 2.2. An incoming sinusoidal TM wave traveling in the x direction will have fields E_z and $-H_y$ for 1/2 of the cycle. These will encounter values of μ_{xy} which are negative in the third quadrant. Equation (2.10) shows that this will result in the generation of positive H_x values. Note that at first there is no variation of E_z with y . This positive H_x field, turns the H field and the wavefront counter-clockwise. In the second quadrant, a negative H_x field is generated which turns the wavefront clockwise. As the wave penetrates deeper into the material, it encounters larger off diagonal values leading to a greater turning tendency. As the wave travels beyond the center, the μ_{xy} signs reverse thus turning the wavefront back. Note that in anisotropic materials, the power flow is not parallel to the normal to the wavefront. [13] The

streamlines of power flow (not shown) bend smoothly around the cylinder. [4]

2.5 Conclusions

With the Yee framework in hand, many other systems can be simulated. Several of these have already been mentioned. A good student exercise is to modify the one dimensional equations (Equ. 2.1 and 2.2) to include materials with finite conductivity to then simulate dissipative systems. Other one dimensional simulations can simulate reflection and transmission at a boundary and anti-reflection coatings. In EPAPS, we provide a one-dimensional Matlab code that would serve well as a starting point. [2] On the 2-D lattice, elementary simulations include refraction of a plane wave, investigation of polarization and Brewster's angle and diffraction from an edge. These and a host of other possibilities are left to the reader to explore.

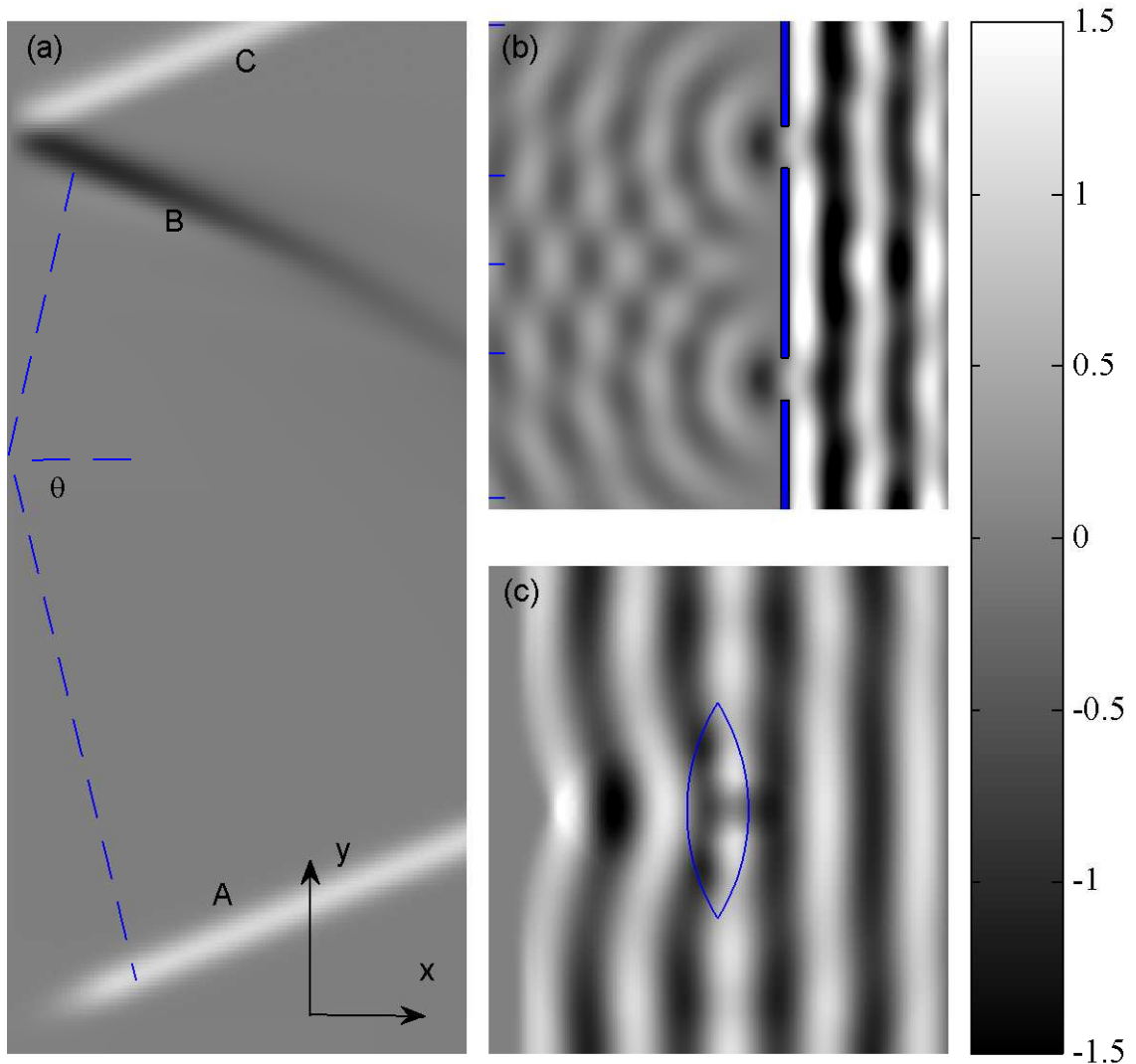


Figure 2.1 Simple optical phenomena arising from Maxwell's equations. The plots show E_z components of the TM waves in our grid with the scale at the right. Note that gray represents zero field and the incident wave has an amplitude of 1.0. A grid of 300×300 is used for each simulation. (a) Simulation of an incident Gaussian pulse reflecting off a perfectly conducting boundary, which is on the left side. (b) Diffraction of a sinusoidal wave through a perfectly conducting double slit. Absorbing boundary conditions are used on the sides in this simulation. (c) Refraction of a sinusoidal wave through a glass converging lens.

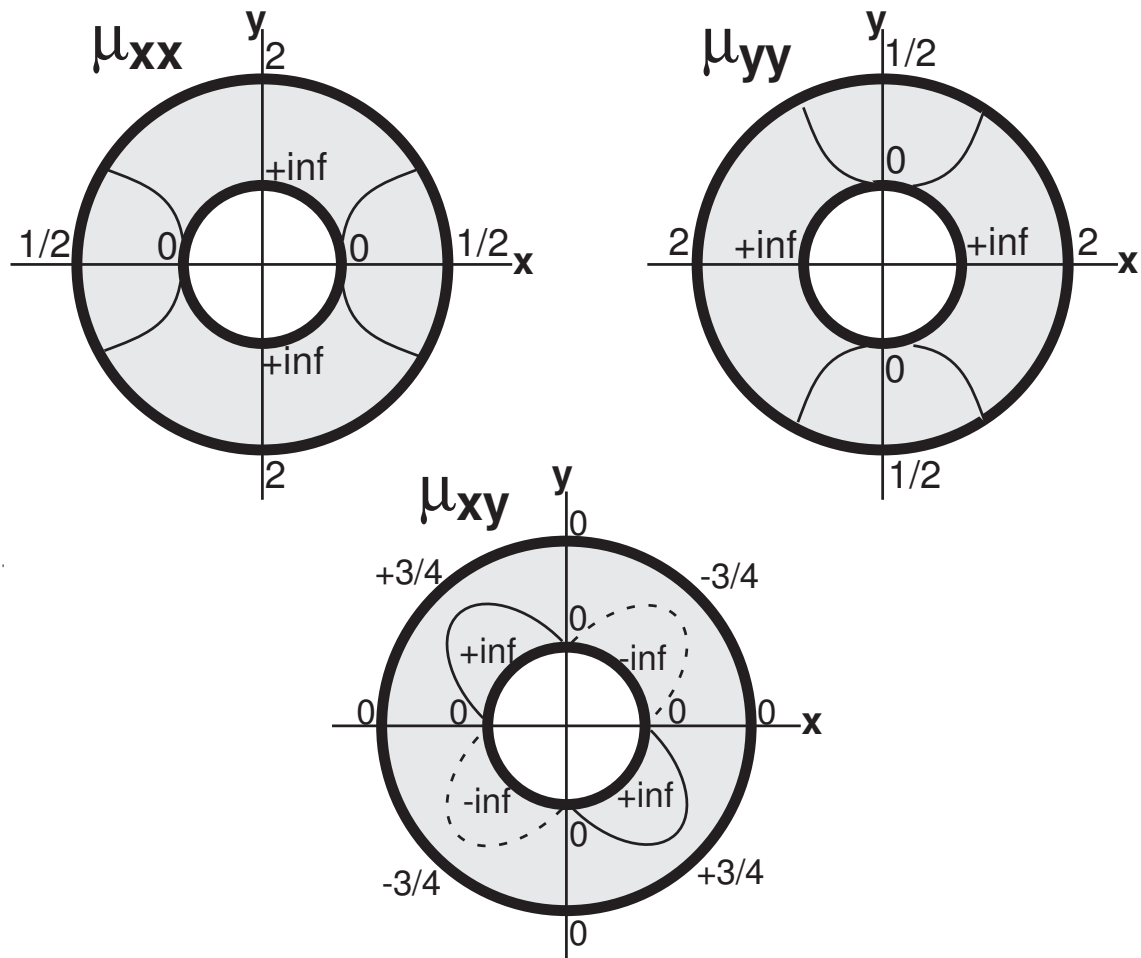


Figure 2.2 Spatial diagrams of the tensor elements, μ_{xx} , μ_{yy} and μ_{xy} , of the permeability material property for bending a TM wavefront around a central region in two dimensions. The numbers indicate the value of the property on the axis at the inner (R_1) or outer (R_2) boundary when the ratio of the boundary diameters is 2. The μ_{xy} diagram includes the values on the diagonal axis. The solid line is a contour for a value of 1.0 and the dashed line is for -1.0. The permittivity property ϵ_{zz} varies from 0 at the inner to +2 at the outer boundary and is symmetric. These properties are calculated for a plane wave inbound from the left.

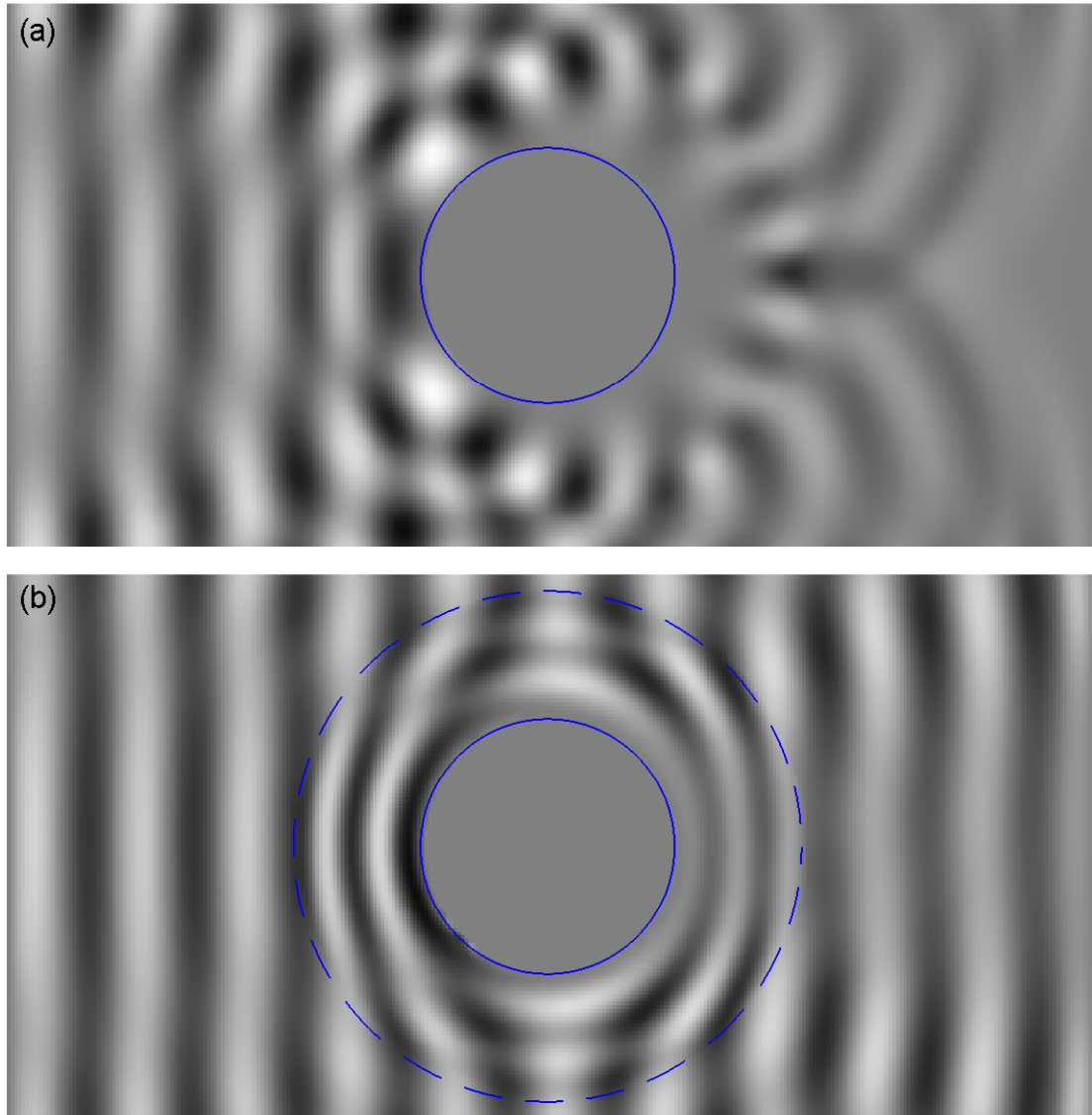


Figure 2.3 Comparison of the scattering of an incident sinusoidal wave **(a)** by a perfectly conducting cylinder of radius R_1 and **(b)** the same cylinder with a concentric cloak of radius $R_2 = 2R_1$. The incident wave is to the right (the $+x$ direction). The shading scale for the electric field is the same as in figure 2.1. Notice that the cloaked cylinder produces some reflection due to the incident wave coming in contact with the cloaked object. This is because of the numerical limiting we apply to μ_{xx} , μ_{yy} and μ_{xy} when r is near R_1 . The videos of these simulations are available in EPAPS. [2]

Appendix A

Yee Algorithm Derivation in 3D

In the cartesian coordinate system, equation 1.1 can be written as

$$\frac{\partial H_x}{\partial t} = \frac{1}{\mu} \left(\frac{\partial E_y}{\partial z} - \frac{\partial E_z}{\partial y} \right), \quad (\text{A.1})$$

$$\frac{\partial H_y}{\partial t} = \frac{1}{\mu} \left(\frac{\partial E_z}{\partial x} - \frac{\partial E_x}{\partial z} \right), \quad (\text{A.2})$$

$$\frac{\partial H_z}{\partial t} = \frac{1}{\mu} \left(\frac{\partial E_x}{\partial y} - \frac{\partial E_y}{\partial x} \right). \quad (\text{A.3})$$

Now, consider the arrangement of field points given in Figure 1.1. Using Yee's notation, Equation A.1 can be written, to first order finite-difference, as

$$\begin{aligned} \frac{H_x^{n+1}(i + \frac{1}{2}, j, k) - H_x^n(i + \frac{1}{2}, j, k)}{\Delta t} = \\ \frac{1}{\mu} \frac{E_y^{n+\frac{1}{2}}(i + \frac{1}{2}, j, k + \frac{1}{2}) - E_y^{n+\frac{1}{2}}(i + \frac{1}{2}, j, k - \frac{1}{2})}{\Delta z} \\ - \frac{1}{\mu} \frac{E_z^{n+\frac{1}{2}}(i + \frac{1}{2}, j + \frac{1}{2}, k) - E_z^{n+\frac{1}{2}}(i + \frac{1}{2}, j - \frac{1}{2}, k)}{\Delta y}. \end{aligned} \quad (\text{A.4})$$

Thus, it follows that

$$\begin{aligned}
H_x^{n+1}(i + \frac{1}{2}, j, k) = & \\
& \left(\frac{\Delta t}{\mu \Delta z} \right) \left(E_y^{n+\frac{1}{2}}(i + \frac{1}{2}, j, k + \frac{1}{2}) - E_y^{n+\frac{1}{2}}(i + \frac{1}{2}, j, k - \frac{1}{2}) \right) \\
& - \left(\frac{\Delta t}{\mu \Delta y} \right) \left(E_z^{n+\frac{1}{2}}(i + \frac{1}{2}, j + \frac{1}{2}, k) - E_z^{n+\frac{1}{2}}(i + \frac{1}{2}, j - \frac{1}{2}, k) \right) \\
& + H_x^n(i + \frac{1}{2}, j, k),
\end{aligned} \tag{A.5}$$

where μ corresponds to the $(i + \frac{1}{2}, j, k)$ point.

In the Cartesian coordinate system, Equation 1.2 can be written as

$$\frac{\partial E_x}{\partial t} = \frac{1}{\varepsilon} \left(\frac{\partial H_z}{\partial y} - \frac{\partial H_y}{\partial z} \right), \tag{A.6}$$

$$\frac{\partial E_y}{\partial t} = \frac{1}{\varepsilon} \left(\frac{\partial H_x}{\partial z} - \frac{\partial H_z}{\partial x} \right), \tag{A.7}$$

$$\frac{\partial E_z}{\partial t} = \frac{1}{\varepsilon} \left(\frac{\partial H_y}{\partial x} - \frac{\partial H_x}{\partial y} \right). \tag{A.8}$$

Then, to first order finite-difference, Equation A.6 can be written as

$$\begin{aligned}
& \frac{E_x^{n+\frac{1}{2}}(i, j + \frac{1}{2}, k + \frac{1}{2}) - E_x^{n-\frac{1}{2}}(i, j + \frac{1}{2}, k + \frac{1}{2})}{\Delta t} = \\
& \frac{1}{\varepsilon} \frac{H_z^n(i, j + 1, k + \frac{1}{2}) - H_z^n(i, j, k + \frac{1}{2})}{\Delta y} \\
& - \frac{1}{\varepsilon} \frac{H_y^n(i, j + \frac{1}{2}, k + 1) - H_y^n(i, j + \frac{1}{2}, k)}{\Delta z}.
\end{aligned} \tag{A.9}$$

Thus, it follows that

$$\begin{aligned}
E_x^{n+\frac{1}{2}}(i, j + \frac{1}{2}, k + \frac{1}{2}) = & \\
& \left(\frac{\Delta t}{\varepsilon \Delta y} \right) \left(H_z^n(i, j + 1, k + \frac{1}{2}) - H_z^n(i, j, k + \frac{1}{2}) \right) \\
& - \left(\frac{\Delta t}{\varepsilon \Delta z} \right) \left(H_y^n(i, j + \frac{1}{2}, k + 1) - H_y^n(i, j + \frac{1}{2}, k) \right) \\
& + E_x^{n-\frac{1}{2}}(i, j + \frac{1}{2}, k + \frac{1}{2}).
\end{aligned} \tag{A.10}$$

Appendix B

Complete Update Equations

Magnetic fields at the next step are defined by:

$$\begin{aligned} H_x^{n+1}(i + \frac{1}{2}, j, k) = & \\ & \left(\frac{\Delta t}{\mu \Delta z} \right) \left(E_y^{n+\frac{1}{2}}(i + \frac{1}{2}, j, k + \frac{1}{2}) - E_y^{n+\frac{1}{2}}(i + \frac{1}{2}, j, k - \frac{1}{2}) \right) \\ & - \left(\frac{\Delta t}{\mu \Delta y} \right) \left(E_z^{n+\frac{1}{2}}(i + \frac{1}{2}, j + \frac{1}{2}, k) - E_z^{n+\frac{1}{2}}(i + \frac{1}{2}, j - \frac{1}{2}, k) \right) \\ & + H_x^n(i + \frac{1}{2}, j, k), \end{aligned} \tag{B.1}$$

$$\begin{aligned} H_y^{n+1}(i, j + \frac{1}{2}, k) = & \\ & \left(\frac{\Delta t}{\mu \Delta x} \right) \left(E_z^{n+\frac{1}{2}}(i + \frac{1}{2}, j + \frac{1}{2}, k) - E_z^{n+\frac{1}{2}}(i - \frac{1}{2}, j + \frac{1}{2}, k) \right) \\ & - \left(\frac{\Delta t}{\mu \Delta z} \right) \left(E_x^{n+\frac{1}{2}}(i, j + \frac{1}{2}, k + \frac{1}{2}) - E_x^{n+\frac{1}{2}}(i, j + \frac{1}{2}, k - \frac{1}{2}) \right) \\ & + H_y^n(i, j + \frac{1}{2}, k), \end{aligned} \tag{B.2}$$

$$\begin{aligned} H_z^{n+1}(i, j, k + \frac{1}{2}) = & \\ & \left(\frac{\Delta t}{\mu \Delta y} \right) \left(E_x^{n+\frac{1}{2}}(i, j + \frac{1}{2}, k + \frac{1}{2}) - E_x^{n+\frac{1}{2}}(i, j - \frac{1}{2}, k + \frac{1}{2}) \right) \\ & - \left(\frac{\Delta t}{\mu \Delta x} \right) \left(E_y^{n+\frac{1}{2}}(i + \frac{1}{2}, j, k + \frac{1}{2}) - E_y^{n+\frac{1}{2}}(i - \frac{1}{2}, j, k + \frac{1}{2}) \right) \\ & + H_z^n(i, j, k + \frac{1}{2}). \end{aligned} \tag{B.3}$$

Electric fields at the next step are defined by:

$$\begin{aligned}
E_x^{n+\frac{1}{2}}(i, j + \frac{1}{2}, k + \frac{1}{2}) = & \\
& \left(\frac{\Delta t}{\varepsilon \Delta y} \right) (H_z^n(i, j + 1, k + \frac{1}{2}) - H_z^n(i, j, k + \frac{1}{2})) \\
& - \left(\frac{\Delta t}{\varepsilon \Delta z} \right) (H_y^n(i, j + \frac{1}{2}, k + 1) - H_y^n(i, j + \frac{1}{2}, k)) \\
& + E_x^{n-\frac{1}{2}}(i, j + \frac{1}{2}, k + \frac{1}{2}).
\end{aligned} \tag{B.4}$$

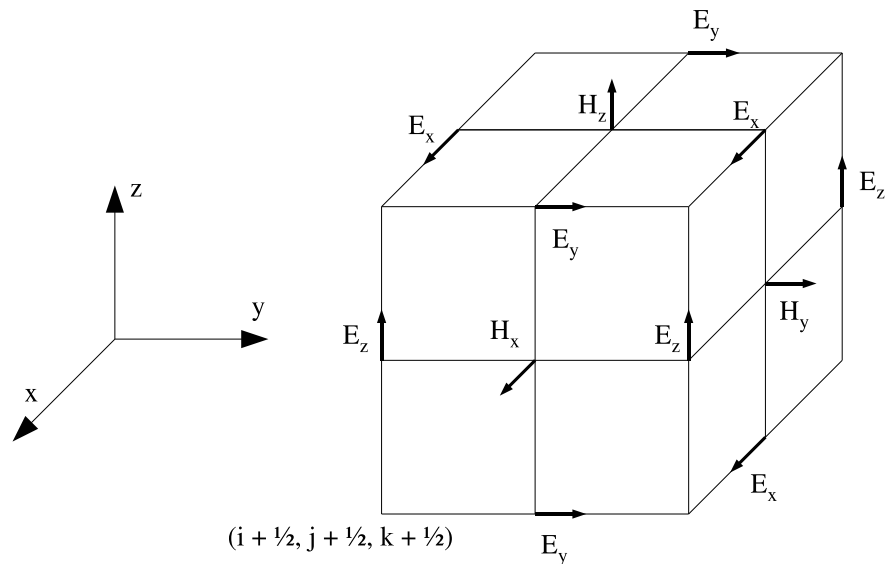
$$\begin{aligned}
E_y^{n+\frac{1}{2}}(i + \frac{1}{2}, j, k + \frac{1}{2}) = & \\
& \left(\frac{\Delta t}{\varepsilon \Delta z} \right) (H_x^n(i + \frac{1}{2}, j, k + 1) - H_x^n(i + \frac{1}{2}, j, k)) \\
& - \left(\frac{\Delta t}{\varepsilon \Delta x} \right) (H_z^n(i + 1, j, k + \frac{1}{2}) - H_z^n(i, j, k + \frac{1}{2})) \\
& + E_y^{n-\frac{1}{2}}(i + \frac{1}{2}, j, k + \frac{1}{2}).
\end{aligned} \tag{B.5}$$

$$\begin{aligned}
E_z^{n+\frac{1}{2}}(i + \frac{1}{2}, j + \frac{1}{2}, k) = & \\
& \left(\frac{\Delta t}{\varepsilon \Delta x} \right) (H_y^n(i + 1, j + \frac{1}{2}, k) - H_y^n(i, j + \frac{1}{2}, k)) \\
& - \left(\frac{\Delta t}{\varepsilon \Delta y} \right) (H_x^n(i + \frac{1}{2}, j + 1, k) - H_x^n(i + \frac{1}{2}, j, k)) \\
& + E_z^{n-\frac{1}{2}}(i + \frac{1}{2}, j + \frac{1}{2}, k).
\end{aligned} \tag{B.6}$$

Appendix C

Divergence Free Nature in 3D

We now show that the Yee's finite-difference formulas implicitly satisfies Equation 1.3. Consider the following Yee cube (cube simply arranged so that the magnetic fields go through the faces):



The total magnetic flux through the faces of the cube can be approximated by

$$\begin{aligned}
\oint_{\text{Yee cube}} \mathbf{H} \cdot d\mathbf{A} = & \\
& (H_x^n(i + \frac{3}{2}, j + 1, k + 1) - H_x^n(i + \frac{1}{2}, j + 1, k + 1)) \Delta y \Delta z \\
& + (H_y^n(i + 1, j + \frac{3}{2}, k + 1) - H_y^n(i + 1, j + \frac{1}{2}, k + 1)) \Delta x \Delta z \\
& + (H_z^n(i + 1, j + 1, k + \frac{3}{2}) - H_z^n(i + 1, j + 1, k + \frac{1}{2})) \Delta x \Delta y.
\end{aligned} \tag{C.1}$$

Now, consider the time derivative of this flux:

$$\begin{aligned}
\frac{\partial}{\partial t} \oint_{\text{Yee cube}} \mathbf{H} \cdot d\mathbf{A} = & \\
& \frac{\partial H_x^n(i + \frac{3}{2}, j + 1, k + 1)}{\partial t} \Delta y \Delta z + \dots
\end{aligned} \tag{C.2}$$

But, we can express the time derivative as a finite difference, as per Equation A.4:

$$\begin{aligned}
\frac{\partial H_x^n(i + \frac{3}{2}, j + 1, k + 1)}{\partial t} \Delta y \Delta z = & \\
\frac{1}{\mu} \left(E_y^{n+\frac{1}{2}}(i + \frac{3}{2}, j + 1, k + \frac{3}{2}) - E_y^{n+\frac{1}{2}}(i + \frac{3}{2}, j + 1, k + \frac{1}{2}) \right) \Delta y & \\
- \frac{1}{\mu} \left(E_z^{n+\frac{1}{2}}(i + \frac{3}{2}, j + \frac{3}{2}, k + 1) - E_z^{n+\frac{1}{2}}(i + \frac{3}{2}, j + \frac{1}{2}, k + 1) \right) \Delta z. &
\end{aligned} \tag{C.3}$$

Once we do this, we find that all of the terms of Equation C.2 end up cancelling:

$$\frac{\partial}{\partial t} \oint_{\text{Yee cube}} \mathbf{H} \cdot d\mathbf{A} = 0. \tag{C.4}$$

Thus, assuming zero initial conditions, the divergence of the magnetic field stays 0.

Bibliography

- [1] K. S. Yee, “Numerical Solution of Initial Boundary Value Problems Involving Maxwell’s Equations in Isotropic Media,” *IEEE Transactions on Antennas and Propagation* **AP-14**, 302-307 (1966).
- [2] See **EPAPS** Document No. E-AJPIAS-76-018803 to obtain the source code used for the simulations, the videos, the one-dimensional spreadsheet and Matlab code. For more information on EPAPS, see <http://www.aip.org/pubservs/epaps.html>.
- [3] A. J. Ward and J. B. Pendry, “Refraction and geometry in Maxwell’s equations,” *J. Mod. Optics* **43**, 773-793 (1996).
- [4] J. B. Pendry, D. Shurig and D. R. Smith, “Controlling Electromagnetic Fields,” *Science* **312**, 1780-1782 (2006)
- [5] G. Mur, “Absorbing Boundary Conditions for the Finite-Difference Approximation of the Time-Domain Electromagnetic-Field Equations,” *IEEE Transactions on Electromagnetic Compatibility* **EMC-23**, 377-382 (1981).
- [6] B. Engquist, A. Majda, “Absorbing Boundary Conditions for the Numerical Simulation of Waves,” *Mathematics of Computation* **31**, 629-651 (1977).

- [7] A. Taflove, M. E. Brodwin, "Numerical Solution of Steady-State Electromagnetic Scattering Problems Using the Time-Dependent Maxwell's Equations," IEEE Transactions on Microwave Theory and Techniques **MTT-23**, 888-896 (1975).
- [8] A. Taflove and S. C. Hagness, eds., *Computational Electrodynamics: The Finite-Difference Time-Domain Method* (Third Edition, Artech House, Boston, 2005).
- [9] Y. Liu, "Fourier analysis of numerical algorithms for the Maxwell's equations," J. Computational Physics **124**, 396-416 (1996)
- [10] J. Schneider and S. Hudson, "The Finite-Difference Time-Domain Method Applied to Anisotropic Material," IEEE Trans. Antennas and Propagation **41**, 994-999 (1993) show the finite difference formulae for tensor conductivity and permittivity but with scalar permeability.
- [11] L. Dou and A. R. Sebak, "3D FDTD Method for Arbitrary Anisotropic Materials," Microwave and Optical Technology Letters **48**, 2083-2090 (2006).
- [12] M. Wilson, "Designer materials render objects nearly invisible to microwaves," Physics Today **60**, 19-23 (2007).
- [13] S. A. Cummer, B. Popa, D. Shurig and D. R. Smith, "Full-wave simulations of electromagnetic cloaking structures," Physical Review E **74**, 036621 (2006).